LAWRENCE
LIVERMORE
NATIONAL
LABORATORY

LLNL-JRNL-401950

Large Eddy Simulation of the Diurnal Cycle in Southeast Pacific Stratocumulus

Peter Caldwell, Chris Bretherton

March 4, 2008

Journal of the Atmospheric Sciences

Disclaimer

Large Eddy Simulation of the Diurnal Cycle in Southeast Pacific Stratocumulus

Peter Caldwell*† and Christopher S. Bretherton

University of Washington, Seattle, Washington

March 7, 2008

*Current Affiliation: Lawrence Livermore National Laboratory, Livermore, CA

†*Corresponding author address:* Peter Caldwell, L-103, Lawrence Livermore National Laboratory, P.O. Box 808, Livermore, CA 94566. E-mail: caldwell19@llnl.gov.

Abstract

This paper describes a series of 6 day large eddy simulations of a deep, sometimes drizzling stratocumulus-topped boundary layer based on forcings from the East Pacific Investigation of Climate (EPIC) 2001 field campaign. The base simulation was found to reproduce the observed mean boundary layer properties quite well. The diurnal cycle of liquid water path was also well captured, although good agreement appears to result partially from compensating errors in the diurnal cycles of cloud base and cloud top due to overentrainment around midday. At other times of the day, entrainment is found to be proportional to the vertically-integrated buoyancy flux. Model stratification matches observations well; turbulence profiles suggest that the boundary layer is always at least somewhat decoupled. Model drizzle appears to be too sensitive to liquid water path and subcloud evaporation appears to be too weak.

Removing the diurnal cycle of subsidence had little effect on simulated cloud albedo. Simulations with changed droplet concentration and drizzle susceptibility showed large liquid water path differences at night, but differences were quite small at midday. Droplet concentration also had a significant impact on entrainment, primarily through droplet sedimentation feedback rather than through drizzle processes.

1 Introduction

Stratocumulus (Sc) cover vast tracts of the midlatitude and eastern subtropical oceans. Their high albedo affects the global top-of-atmosphere radiation balance (Klein and Hartmann, 1993), cools the underlying ocean (Nigam, 1997), strengthens the subtropical highs, and affects the tropical rainfall belts (Yu and Mechoso, 1999). Sc are also among the worst-simulated tropical clouds in general circulation models (GCMs) (Bony and Dufresne, 2005). Large observational uncertainties remain in some important characteristics of Sc-topped boundary layers, especially entrainment rate and drizzle processes.

One reason these clouds are hard to simulate is that key processes in Sc occur on scales much thinner than a GCM grid cell so must be parameterized, but parameterization is difficult because these processes interact in a very complicated and sensitive way. Additionally, lack of reliable observational data near the top of Sc adds to the challenge of formulating and evaluating parameterizations.

Large eddy simulation (LES) has become a popular tool for investigating Sc because it explicitly resolves the motions thought to be important for the Sc-topped boundary layer (BL), thus (at least in principle) circumventing the need for uncertain parameterizations. Because LES provides easy access to information which is difficult or impossible to measure observationally, these simulations are often used as a source of "synthetic observations" for developing large-scale model parameterizations (e.g. Lewellen and Lewellen, 1998; Lock, 1998; vanZanten et al., 1999; Moeng, 2000). LES is particularly well suited for investigating the effect of individual forcings on BL behavior, a task which is fre-

quently impossible from observations (since all forcings tend to vary in concert). These simulations are not without problems, though. One issue is that the computational power needed to resolve the range of Sc-relevant scales exceeds the capacity of many modeling centers and severely limits the number of simulations which can be run. Another issue is that it is still unclear whether LES provides a realistic depiction of Sc at all. This last issue is the focus of a series of model intercomparison studies organized under the auspices of the GEWEX Cloud System Study BL cloud working group. The results of these studies suggest that model results are frequently quite poor, but that good simulations are possible if care is taken to limit subgrid-scale fluxes across the inversion(Stevens et al., 2005b, and references therein).

The first goal of this study is to examine the extent to which LES is able to reproduce the conditions observed during the East Pacific Investigation of Climate (EPIC) 2001 field campaign (Bretherton et al., 2004). The Sc component of EPIC, which took place between Oct 16-21, 2001 at 20° S, 85° W, was the first to adequately sample multiple diurnal cycles in a pristine marine Sc environment. As such, it provides a great opportunity for testing the ability of LES to simulate the entire diurnal cycle. Since Sc affect the Earth's energy budget chiefly through reflection of solar radiation, correct simulation during the day is arguably more important than at night, yet most previous observations and simulations have been nocturnal, when forcing is steadier. Additionally, ability to model the BL response across the entire diurnal cycle provides confidence that model response to perturbations will be correct, something that cannot be tested

from steady-state runs alone. Once satisfied that the model is a reasonable surrogate for reality, we focus on the remaining goals of the study - using our control simulation to investigate BL properties not measured during EPIC and using sensitivity runs to test the importance of the various forcings to model behavior.

In the following two sections, we describe our model formulation and experimental design. Section 4.1 follows with validation of model results against the EPIC observations. Section 4.2 then explores the model's turbulent kinetic energy (TKE) budgets (where observational data is not available) and section 4.3 analyzes model entrainment and what it suggests for large-scale parameterization. This is followed by sensitivity studies in sections 4.4 and 4.5 and conclusions in section 5.

2 Model Formulation

The LES model we use for this study is the System for Atmospheric Modeling (SAM, Khairoutdinov and Randall, 2003) version 6.5. This is an anelastic model based on prognostic equations for precipitating and non-precipitating water mixing ratio (q_l and q_t, respectively), and liquid water static energy (s_l). Our version is modified to use the Khairoutdinov and Kogan (2000) (hereafter KK) drizzle parameterization with fixed droplet concentration N_d, requiring an additional prognostic equation for drizzle drop concentration. Effective radius (used for radiative transfer) is computed from N_d and liquid water path (LWP) at each grid cell following Martin et al. (1994). Radiative fluxes are computed every 20 timesteps using the CAM3 radiation code (Collins et al., 2006)

with time-varying zenith angle computed to match conditions during the EPIC cruise. A model timestep of 4 sec is imposed, though each step is broken by the model into smaller substeps as needed in order to maintain stability. Our domain is taken to be doubly periodic in the horizontal directions with a sponge layer occupying the top 30% of our domain.

Surface fluxes were computed from local wind speed and thermodynamic properties at the lowest grid point (2.5 m) following Monin-Obukhov theory. The Coriolis force is computed from geostrophic winds (assumed equal to EPIC radiosonde winds in the free troposphere and ramping linearly to a surface value computed as described in appendix 5). To keep surface winds (and hence surface fluxes) close to observed values, we nudge winds to the observations using a timescale which increases smoothly from 100 min near the surface to one day above the domain-mean inversion height. By nudging winds even in the free-troposphere where they are close to geostrophic, we damp inertial oscillations that may otherwise be excited as the winds change.

As noted in Stevens et al. (2005b), correct entrainment rates are a prerequisite for accurate simulation of the Sc-topped BL. However, they are hard to obtain, even with a high-resolution LES. Bretherton et al. (1999) find high vertical resolution around cloud top ($\leq$ 5 m) to be necessary in order to control overentrainment due to spurious numerical diffusion. In order to provide high resolution at cloud top while minimizing computational cost, we use a vertically-stretched grid with a minimum grid spacing of 5 m near the surface and inversion and larger grid spacing (up to 50 m) elsewhere (Fig.

1). To further decrease computational expense, we employ a relatively large (25 m) horizontal grid spacing. This is a reasonable tactic since studies using a variety of advection and subgrid turbulence schemes (Lewellen and Lewellen, 1998; Stevens et al., 1999) have found entrainment to be relatively insensitive to horizontal grid spacing. One study which did obtain dependence on horizontal grid size (Stevens and Bretherton, 1999) found entrainment to decrease slightly with coarsening horizontal resolution. If this last study is correct, increasing grid anisotropy may actually be a way to compensate for the typical LES overprediction of entrainment (w_e). A sensitivity test (section 4.4) suggests that decreasing horizontal resolution does not significantly affect entrainment in SAM.

Creating an LES simulation of Sc which produces realistic entrainment also requires using a subgrid-scale (SGS) parameterization which limits mixing across the inversion (Stevens et al., 2005b). While this occurs naturally for dynamic SGS models (e.g. Germano et al., 1991), these models are complicated, computationally intensive, and involve assumptions which are hard to justify physically (Pope, 2000, p.626) and are therefore not widely used. More typical atmospheric SGS parameterizations such as that of Smagorinsky (1963) and Deardorff (1980) (both available in SAM), however, tend to produce too much mixing across the inversion. Stevens et al. (2005b) found that for a nocturnal Sc simulation with the UCLA LES, simply turning off the SGS model for scalars resulted in good agreement with observations. We follow this procedure for our runs, though a sensitivity study presented in section 4 suggests that this omission makes very little difference to our simulations. For momentum, we apply the Smagorinsky SGS

scheme with horizontal diffusivity scaled by $(\Delta x/\Delta z)^2$ (where Δx is the horizontal grid spacing and Δz is the vertical grid spacing) to account for the large anisotropy of our grid.

Ackerman et al. (2004) found entrainment to be significantly decreased by cloud droplet sedimentation. This is explained in Bretherton et al. (2007) as a consequence of removing liquid water in the cloud-top region, which decreases evaporative enhancement in entraining plumes and (to a lesser extent) decreases cloud-top radiative cooling. Sedimentation is included in SAM following equation 7 of Ackerman et al. (2008), which assumes cloud droplets are log-normally distributed with geometric standard deviation σ_g and fall at a rate given by Stokes' law. While observational evidence suggests σ_g should be between 1.2 and 1.5, we use this quantity as a tuning parameter to keep our model from overentraining. We find that $\sigma_g = 2.0$ provides reasonable results for 3D simulations while $\sigma_g = 1.9$ is optimal for 2D cases.

The difficulty of simulating the diurnal cycle of Sc with LES is evident from the dearth of such studies in the literature. Duynkerke et al. (2004), the one study we are aware of which simulated the diurnal cycle of Sc, resorted to tuning the subsidence rate to compensate for overentrainment, resulting in simulated BLs which were too dry and warm.

An obvious challenge with a study of the diurnal cycle is that it requires relatively long model runs. In order to achieve the required spatial resolution yet keep these runs computationally feasible, either the domain size or the dimensionality must be limited.

One compromise we make is to perform our sensitivity studies with 2D simulations. These simpler simulations are shown in section 4 to behave quite similarly to their 3D analogues. Our runs use 128 grid points in the horizontal direction(s) and 272 grid points in the vertical, resulting in a domain size of 3.2 km (horizontal) by 2.2 km (vertical). At this resolution, a 3D 6-day simulation on 16 nodes of our Linux cluster takes about 100 hours. Each node of this cluster consists of 2 dual-core Opteron 2210 (1.8GHz) processors for a total of 64 cores per simulation.

A 3.2 km wide domain is too small to resolve multiple convective cells, so our simulation typically includes just one domain-filling cell at a time (Fig. 2). While one cell is obviously not enough to use for statistical analysis, our simulations are long enough that temporal variations can, to some extent, make up for the lack of spatial resolution. To this effect, all model data is averaged up to 3 hr resolution for analysis unless otherwise noted. A larger question is whether our limited domain properly handles the effect of drizzle, which is thought to induce mesoscale BL organization with potentially important repercussions for domain-mean properties (e.g. Paluch and Lenschow, 1991; Stevens et al., 2005a). While this question has not been answered definitively, comparison of 6.4×6.4 km and 12.4×12.4 km simulations in Xue et al. (2007) show little difference in domain-mean quantities, even though mesoscale variability is much enhanced in the larger-domain simulation. Additionally, the 25×25 km simulations of Savic-Jovcic and Stevens (2007) show qualitatively the same drizzle response as similar simulations performed by Stevens et al. (1998) on a domain comparable to ours. In section 4 we do a 2D

sensitivity study which suggests that domain size has only minor effect on our results.

Another problem with long simulations is that large-scale processes typically omitted from LES become important. In particular, horizontal advection should be height-independent in the BL for well-mixed conditions, but may change discontinuously across cloud top. Since available advective forcings are relatively uncertain and don't resolve the inversion very well, and because the depth of the BL changes in time and across columns, it is easier and more accurate for us to apply height-independent BL advections to the whole model domain, and then to correct for this anomalous forcing by nudging free tropospheric θ_l and q_t towards the EPIC radiosonde profiles with a relatively short (3 hr) relaxation timescale. This procedure is essentially the same as that employed in deSzoeke and Bretherton (2004). Because nudging in the entrainment zone would artificially affect the entrainment process, we start nudging 75 m above the domain-averaged value of boundary-layer depth z_i (computed as the height of most negative domain-averaged $\partial q_t/\partial z$). A buffer depth of 75 m was chosen because it is the smallest depth which is always larger than the thickness of the region of significant q_t gradient in our simulations.

3 Initialization and Forcing

We initialize and force the model with data from the EPIC Sc dataset, which is publicly available at www.atmos.washington.edu/∼breth/EPIC/EPIC2001_Sc_ID/sc_integ_data_fr.htm. In order to avoid nudging the modeled free-troposphere toward BL values when the model's z_i falls below that of the observations, we replace the BL component of the

input θ_l and q_t profiles with data interpolated linearly from the overlying soundings. We use ECMWF values for w_s and advection of θ_l and q_t instead of NCEP values because ECMWF was found to be more believable in C05. The dataset only includes subsidence at 850 mb, so we construct profiles by assuming w_s increases linearly with height from a surface value of zero. Profiles of advection and subsidence are included in Fig. 3. Note that the forcings are actually quite variable in time and that w_s has a very regular diurnal cycle with strongest subsidence around local noon and periods of mean upward motion around midnight. In C05, diurnal variations in subsidence and entrainment were found to contribute roughly equally to the large observed diurnal cycle of z_i; a major goal of this study is to determine the importance of w_s variations in an environment that can react dynamically to forcing changes. The time-series of z_i advection is absorbed into the subsidence by adding $-\mathbf{v} \cdot \nabla_h z_i = -0.49\text{mm s}^{-1}$ (taken from C05) to w_s(850 mb) before creating profiles. Estimates of N_d are included in the EPIC dataset, but are quite uncertain. For this reason and to simplify comparisons, most of our simulations were performed at fixed droplet concentration.

4 Results

4.1 Validation

Our base run is a 3D simulation with fixed $N_d = 100$ cm^{-3}. Tables 1 and 2 compare the 6-day mean q_t and s_l budgets from this simulation with those derived in C05. The overall agreement is quite impressive, but we note that these budgets are strongly controlled

by the mean entrainment rate, which has been tuned using σ_g to match observations. Modeled entrainment fluxes are slightly overestimated, which results in a drier BL and causes a slight increase in modeled LHF over observations. Radiative cooling is somewhat underestimated because model LWP is underpredicted.

The timeseries of modeled LWP is compared to the EPIC observations in Fig. 4a. Aside from day 293, the model does a reasonable job of reproducing the observed LWP timeseries, albeit with a bias toward low values. In particular, this run captures the observed diurnal variability in LWP very well, suggesting that sensitivity studies with SAM are a useful tool for better understanding the variations sampled during EPIC. Model cloud fraction is frequently lower than observed (Fig. 4b).

The strong decrease in LWP and cloud fraction around day 293 appears to be due to the combination of strong dry advection and weak cold advection which begins on day 292 (Fig. 3). Simulations using 6-day mean advections (not shown) did not show this decrease around day 292-293, but were unsuitable for analysis because they had much thinner clouds in general.

Fig. 5a shows the timeseries of modeled and observed surface drizzle. The model appears to capture drizzle events fairly well in all cases except during the previously discussed period between day 292 and 293, but with a tendency towards premature initiation. Additionally, the strength of surface precipitation is significantly overestimated by the model. Both early initiation and overprediction suggest that the drizzle scheme is too sensitive to LWP. This hypothesis is substantiated in Fig. 5b, which shows the

relation between cloud base drizzle $F_P(z_b)$ and LWP/N_d. Since both axes on this plot are log-scaled, straight lines on this graph denote a relation of the form

$$F_P(z_b) = A\left[\frac{\text{LWP}}{N_d}\right]^B \tag{1}$$

where A and B are the line's y-intercept and slope, respectively. The best-fit line to mm-wavelength vertically pointing radar from EPIC (derived in Comstock et al., 2004) has $A = 0.0156$ and $B = 1.75$ and is included in this figure as a black dashed line. The best-fit relation from SAM data, on the other hand, takes $A = 0.007$ and $B = 3.58$. Clearly, the KK scheme is much more sensitive to LWP[1] than expected from the EPIC data. Similarly, the relationship between $F_P(z_b)$ and cloud thickness in our simulation is stronger than found in previous studies (e.g. Pawlowska H. and J.-L. Brenguier, 2003; Vanzanten et al., 2005; Wood, 2005). Part of this discrepancy may result from the fact that drizzle increases nonlinearly with LWP, so A and B will be decreased when $F_P(z_b)$ and LWP are averaged over non-drizzly regions. The model A and B are based on data averaged over the domain and over 20 min intervals (longer averaging doesn't change the results), while the Comstock et al. (2004) relationship is based on 3 hr averages from a single spatial point. As a result, it is difficult to disentangle which is "more averaged". On the other hand, the small domain size of the model may be preventing regions of intermediate LWP (and hence lower $F_P(z_b)$) from forming, which would artificially increase A and B. It should also be noted that (as in all radar precipitation retrievals) there is substantial uncertainty in the Comstock et al. (2004) parameterization. Evidence

[1] N_d sensitivity can't be tested here since N_d is fixed at 100 cm^{-3} in this run.

of this can be found in Fig. 5b by noting that the scanning cm-wavelength data don't follow the same slope as the Comstock et al. (2004) line, which was computed by sampling the same clouds, but with a mm-wavelength vertically-pointing radar.

The timeseries of q_l, z_i, z_b, and 15m lifting condensation level (LCL) from the base simulation are compared with the observations in Fig. 6. As expected for well-mixed Sc, the modeled liquid water content increases smoothly with height and there is no sign of scud or cumulus detraining into the Sc. Peak q_l is relatively modest at around 0.5 g kg^{-1}. The modeled cloud-top height matches the observations quite well in the mean, but underestimates the diurnal cycle (panel (b)). Since entrainment is directly related to cloud-top evolution through the equation

$$\frac{\partial z_i}{\partial t} + \mathbf{v} \cdot \nabla_h z_i = w_e + w_s(z_i) \tag{2}$$

and $\mathbf{v} \cdot \nabla_h z_i$ and w_s are forced in the model from observations, this implies that the model is reproducing the mean entrainment rate, but is underpredicting its diurnal amplitude relative to the observations. The question of whether this reflects an error in the model or in the observations is examined further in section 4.3.

For this study, cloud base is taken as the domain-median value from each 3D output timestep for consistency with the methodology of the observations. While the observed cloud base remains approximately constant throughout the study period, the modeled z_b tends to rise during the day and descend at night. This is probably due to extra entrainment warming and drying in the model during the day and enhanced entrainment cooling and moistening at night. Interestingly, model/observation agreement in LWP is

improved by cancellation of z_i and z_b errors. This cancellation emphasizes the necessity of using multiple metrics for assessing model performance.

Also included in Fig. 6 are observed and modeled LCL. The difference in composite diurnal cycle LCL between model and observations is again consistent with larger daytime entrainment in the model. While the observed LCL drops during the day in response to decreased entrainment (as described in C05), the modeled LCL (which sees much steadier entrainment) remains constant. The difference between LCL and cloud base is useful as a measure of BL stratification and therefore mixing between the cloud layer and the near-surface air. The fact that this difference is approximately the same in both model and observations suggests that both experience about the same level of mixing. Extensive comparison of modeled and observed q_t and s_l stratification (not shown) support this conclusion.

4.2 Turbulent Structure

To the extent that our LES simulation parallels reality, it provides us with a wealth of data fields not sampled during the EPIC cruise. With this data, we can investigate a variety of questions which would be intractable based on the observations alone. One such question is what determines the degree of stratification found in the EPIC BL. Since vertical velocity variance ($\overline{w'w'}$) measures the strength of the turbulent motions which mix the BL, examination of this quantity is a natural starting point. Profiles of $\overline{w'w'}$ averaged over each 3-hr period of the simulation and grouped by day are plotted

in Fig. 7. Unsurprisingly, $\overline{w'w'}$ is weaker during the day (gray lines) than at night (black lines). This is the result of decreased daytime cloud-top radiative cooling due to SW absorption. More interestingly, almost all $\overline{w'w'}$ profiles show a bimodal structure with a distinct minimum in the middle of the BL. This indicates that even at night the BL is not fully coupled. At some point comparison with observed $\overline{w'w'}$ below cloud base should be possible based on vertical air velocity measurements from a NOAA ETL upward-pointing Doppler lidar which was operating during the cruise, but this data is yet to be processed.

An odd feature of Fig. 7 is that the subcloud peak in $\overline{w'w'}$ is often larger than the cloudy peak. This behavior seems to be associated with convective bursts which may be an artifact of our small domain size. These pulses are buoyancy-driven and are easily visible against a background state of near-zero subcloud buoyancy flux ($\overline{w'b'}$) in Fig. 8a. Aside from these pulses, the BL shows the top-heavy $\overline{w'b'}$ structure typically found in these clouds. Buoyancy flux is much stronger during nighttime hours (indicated by black lines at the bottom of the plot), and almost dies out completely during daylight hours. The model fails to capture the pre-dawn decrease in subcloud $\overline{w'b'}$ noted in C05. This is unsurprising because the pre-dawn decrease was hypothesized to result from the observed early-morning peak in drizzle which is not present in the model (Fig. 5a).

The remaining terms in the BL TKE budget are included in panels (b)-(d) of Fig. 8. In accordance with expectations, $\overline{w'b'}$ is seen to be the dominant source of TKE away from the surface layer. Nonetheless, shear does occasionally play an important role near

the surface when turbulence (and therefore the potential for wind shear) is strong. It is possible that our nudging procedure is artificially enhancing shear, but since shear is relatively small this is probably not a major concern. An odd and unexplained feature of this simulation is that the TKE generated in the cloud layer by buoyancy flux is not generally dissipated in situ, but rather transported downward and removed near the surface. This is in contrast to LES of shallower marine Sc layers, which show substantial TKE dissipation in the cloud layer (e.g. the intercomparison by Stevens et al., 2005b).

4.3 Entrainment

In addition to controlling the degree of mixing in the BL, turbulence determines entrainment. Evidence of this is found in Fig. 9a, which compares model entrainment[2] to the vertical velocity variance at $0.9\, z_i$. The extremely tight correlation between these quantities suggests that entrainment in SAM is driven by eddies rather than numerical diffusion. Weaker turbulence during the night results in lower entrainment rates during the day (light dots) than at night (dark dots).

For turbulence-based entrainment parameterization, one must also predict any turbulence statistics (e.g. $\overline{w'w'}$) used to deduce the entrainment. It is often simpler to predict the energy source for the turbulence (typically the buoyancy flux in convective boundary layers), and relate the entrainment rate to this. Several such parameterizations were compared in Stevens (2002) and C05. The most basic of these, which simply relates entrainment to the buoyancy driving (given by $w_* \mathrm{Ri}^{-1} = w_*^3/(\Delta b z_i)$ with

[2]computed as the residual of the mass budget (2).

$w_*^3 = 2.5 \int_0^{z_i} \overline{w'b'} dz$) was found in the latter of these studies to match the observations quite well, with slope $A = w_e \mathrm{Ri}/w_*$ of 1.1. In Fig. 9b, this analysis is repeated for the LES data. The model fit to the data is quite good (correlation 0.76) and the least-squares slope (constrained to pass through the origin) of $A = 1.0$ is almost indistinguishable from that of the observations. Such agreement is quite surprising in light of the model's apparent inability to reproduce the observed diurnal cycle of entrainment.

This mystery is investigated further in Fig. 10, which compares the diurnal cycle of $w_* \mathrm{Ri}^{-1}$ and w_e for model and observations. As expected on the basis of Fig. 9b, $w_* \mathrm{Ri}^{-1}$ is a good predictor of entrainment most of the time. In fact, we see that the diurnal amplitude of model w_e is only too weak because of the single very low value of observed w_e at 1100 LT. This time is also the only point on this figure which doesn't obey the $w_* \mathrm{Ri}^{-1}$ scaling.

There are two possibilities for why the observed 1100 LT point doesn't match this scaling. One possibility is that some sort of regime transition is occurring around midday, during which time entrainment is limited by some other process. Since it is hard to imagine what that process may be, this option seems unlikely. The other possibility is that the 1100 LT point from the mass budget is wrong. This must be somewhat the case since the midday entrainment observation is negative, which is unphysical. Further, partial decoupling is likely around midday, making the observed w_* for this time (computed assuming well-mixed conditions) relatively uncertain. At first glance, the discrepancy between modeled and observed diurnal amplitude in z_i appears to provide

independent verification that it is the model which is wrong. This is not the case since the observed w_e was derived from relation (2) and the model was forced with the same $w_s - \mathbf{v} \cdot \nabla_h z_i$ as used in the mass budget, making disagreement about the diurnal cycle of w_e a direct consequence of the disagreement in z_i. It is possible that the observed midday z_i is underpredicted since the difference between cloud top and BL top increases during the day (making it difficult to accurately assess z_i) and because the uncertainty implicit in determining z_i from a single radiosonde profile every three hours is substantial. Nonetheless, all three independent budgets support the notion that entrainment is lower around midday than predicted by the LES.

It should be noted that good model-observation agreement in entrainment efficiency A is potentially the result of tuning σ_g. Without this tuning, the entrainment efficiency would likely be much higher. Still, tuning is unlikely to affect the impressively tight correlation between w_e and $w_* \mathrm{Ri}^{-1}$ found in the model.

Additionally, tuning σ_g may actually be artificially damping the diurnal cycle of w_e since the effectiveness of σ_g damping is proportional to the amount of liquid water at cloud top, which is much higher at night (when entrainment should be high). An alternative technique for dealing with overentrainment (employed in Duynkerke et al., 2004) is to allow entrainment to evolve freely while tuning w_s to keep z_i in check. We performed a 2D sensitivity study employing this technique and did find it to increase the diurnal cycle of z_i by about 100 m over the first day (compared to a 2D base simulation). Unfortunately, allowing the model to overentrain causes the BL to dry and warm, resulting

in a complete loss of cloud after 2 days of simulation. How to optimally deal with model overentrainment is a question which becomes increasingly important as LES are run for longer periods. Obviously, using a model which correctly simulates entrainment would be ideal. Increasing vertical resolution beyond 5 m may be a step in this direction, but this would add considerable expense to simulations which are already computationally taxing. In the absence of a perfect model, one must choose between techniques which artificially influence the entrainment process and those which attempt to correct for overentrainment by changing forcings. Determining the best way to do this is an important problem for future studies.

Another interesting feature of Fig. 10 is the timing of the diurnal cycle of entrainment, which appears to be shifted about 3 hours later in the LES. Since the onset of decreased turbulence in the observations is theorized to result from an early-morning drizzle maximum absent in the model (which instead drizzles all night, Fig. 5a), this shift is perhaps unsurprising. Additionally, the 3 hr delay in the upswing of model w_e is consistent with the fact that more spin-up time is required to restore mixing to the almost cloud-free BL found in the model in late afternoon (Fig. 4). Another possibility is that the timing of the observed mass budget is wrong since entrainment from the s_l and q_t budget w_e show a lag similar to the model (C05, Fig. 5).

The typical lengthscale of eddies driving entrainment is still unclear. Some studies (such as Lewellen and Lewellen, 1998) theorize the that entrainment rate adjusts to remove a certain fraction of BL-integrated buoyancy production, while others (e.g. Lilly,

2002) theorize that the entrainment rate depends on the vertical structure and vigor of the large eddies that actually impinge on the entrainment interface. We investigate this issue in Fig. 11 by looking at the correlation between turbulence and entrainment as a function of height. Unsurprisingly, entrainment is better correlated to vertical velocity variance (panel a), than to buoyancy flux (panel b) or buoyant forcing (Fig. 9b) since $\overline{w'w'}$ measures the motions responsible for entrainment while $\overline{w'b'}$ measures the energy source for these motions. Better understanding of the transfer function relating these two quantities would be very useful for improving entrainment parameterizations, but is outside the scope of this research. The extremely high correlation with vertical motions in the top 60-90% of the BL (as well as the double-peaked structure of vertical velocity variance, which suggests a separation of the eddy structures in the surface and cloud layers) suggests that the vertical motions responsible for entrainment have lengthscale less than 40% of the BL depth. This implies that Lilly's approach of weighting turbulence generation near cloud-top more heavily than near the surface is probably preferable to the w_* approach of Turton and Nicholls (1987).

4.4 Sensitivity to Model Configuration

The impact of our various modeling assumptions is compared in Fig. 12, which shows timeseries of z_i, z_b, and LCL for various run configurations. In panel (a), results from a 2D base simulation are compared with those from the 3D base simulation discussed above. This comparison is important because, as noted in section 1, we lack the computational

resources to do all of our sensitivity studies in 3D. Agreement between the two runs is quite good until day 292, when the cloud essentially disappears from both simulations (due, as noted in section 4.1, to advection). While cloud rapidly reforms in the 3D simulation, the 2D run remains cloud free, which causes the BL to collapse due to a lack of cloud-top radiative cooling. The reason for this differing behavior is unclear, but could be related to the ability of the 3D simulation to store more TKE in horizontal motions. This may result in a slower TKE loss rate and hence provide enough residual mixing to allow for reformation of cloud once the warm/dry advection spike passes. Another noteworthy difference between the 2D and 3D runs is the entrainment rate. While z_i (and thus entrainment) is approximately the same for the initial cloudy days of both runs, σ_g had to be slightly decreased to 1.9 in order to achieve this agreement. When σ_g is kept at 2.0, 2D runs underentrain significantly. The reasons for this are still unclear. The 2D case seems to have slightly less diurnal variation in z_i and thus w_e, again for reasons unknown.

The effect of increasing domain size on 2D simulations is investigated in panel (b). The larger domain run entrains slightly less (perhaps because pulses of $\overline{w'b'}$ are less common), resulting in slightly lower average LCL and z_b than found in the 2D base simulation. Nonetheless, model behavior in the large-domain simulation is qualitatively similar to that from the base run, suggesting that increased domain size is unlikely to change our results. Similarly, decreasing horizontal grid spacing from 25 m to 6.25 m causes entrainment and drizzle to decrease slightly, but otherwise makes little difference.

This sensitivity is in the opposite sense as found in Stevens and Bretherton (1999), perhaps due to our use of an anisotropic eddy diffusivity.

Finally, model sensitivity to use of the Smagorinsky SGS scheme for computing scalar fluxes is considered in panel (d). Differences in model behavior are almost imperceptible, leading us to conclude that inclusion of a SGS scheme for scalars neither helps nor hurts our simulation, a striking difference from the results reported in Stevens et al. (2005b) for the UCLA LES.

4.5 Sensitivity to Model Microphysics and Forcings

A great benefit of LES studies is that the effect of individual forcings can be isolated in a physically-consistent setting by repeating the control simulation with the forcing of interest changed. In Fig. 13 we use this technique to investigate the effect of diurnally-varying subsidence. In panel (a), we see that removing the diurnal cycle of subsidence results in a simulation with very little variation in z_i on the timescale of a day. If the real diurnal cycle of w_e is closer to the model-predicted value than to the observations as discussed in section 4.3, this implies that subsidence is largely responsible for the observed diurnal cycle in cloud top. In the sensitivity simulation, decreases in cloud base generally make up for damped variation in z_i, resulting in little change to the LWP. Other BL quantities, such as drizzle, surface fluxes, and mixing are quite similar for both simulations (not shown).

The effect of drizzle on the simulations is examined in Fig. 14. Four cases are consid-

ered: drizzly cases with N_d fixed at 100 cm^{-3} and N_d fixed at 25 cm^{-3}, and companion runs at each of these droplet concentrations where drizzle has been artificially suppressed by turning off autoconversion. The drizzly run at $N_d = 100$ cm^{-3} only precipitates intermittently (panel (a)), while precipitation is frequent and substantial at $N_d = 25$ cm^{-3}. Interestingly, while the low-N_d case typically has much higher surface precipitation than the observations, cloud base drizzle is frequently higher in the observations than in of any of the simulations. This suggests that the model underpredicts evaporation of falling droplets, perhaps because it neglects ventilation. Oddly though, SAM overpredicted the fraction of drizzle evaporated below cloud in the shallower RF02 case (Ackerman et al., 2008). Early initiation of drizzle (compared to observations) is apparent in both the $N_d = 25$ cm^{-3} and $N_d = 100$ cm^{-3} simulations.

Panel (b) shows that increasing drizzle susceptibility causes a strong decrease in daily-maximum LWP, but has little effect on the daily minimum (daytime) LWP. This appears to be due to LWP falling to such low values during the day that drizzle can't be sustained in any simulation (panel (a)), in which case model physics is essentially identical for all simulations until night falls and the LWP picks up again. Panel (c) shows that the non-drizzly simulation can nevertheless result in an enhancement of the shortwave cloud forcing of over 100 W m^{-2} relative to the heavily drizzling case due to the Twomey effect and to enhanced LWP during morning and evening hours.

Panel (d) shows that cloud fraction is essentially the same in all 4 simulations until the disappearance of cloud on day 293. This is somewhat surprising since the average

LWP in the heavily drizzling simulation is half that in the non-drizzly case.

Perhaps the most interesting feature of this graphic is that the response of model z_i (and thus w_e) to N_d changes seems to be entirely unrelated to drizzle processes (panel (e)). Further runs with both drizzle and cloud droplet sedimentation turned off did not exhibit N_d dependence (not shown), which leads us to conclude that entrainment in our simulations is controlled entirely through cloud droplet sedimentation. It should be noted that the importance of cloud droplet sedimentation is enhanced in our simulations by artificially increasing σ_g. Subsequent runs with $\sigma_g = 1.2$ (Fig. 15) show more sensitivity to drizzle, but sedimentation still seems to dominate[3]. In light of our results it seems inappropriate to associate entrainment response to N_d with drizzle processes as commonly assumed (e.g. Savic-Jovcic and Stevens, 2007).

The importance of sedimentation is echoed in an LES intercomparison study by Ackerman et al. (2008), which found LWP to increase in almost all models when sedimentation and drizzle were included. Since drizzle by itself acted to decrease LWP in almost all simulations while sedimentation by itself acted to increase LWP, LWP enhancement when both effects were included was taken as a sign that sedimentation was more important (at least for their case). The effect of sedimentation on z_i was not considered in their study. While our study parallels Ackerman et al. (2008) in concluding that sedimentation is more important than previously thought, results here differ in that we find LWP to *decrease* when sedimentation is increased. This is perhaps due to decreased

[3]The counter-intuitively higher z_i values for N_d=25 cm^{-3} simulations in this graphic are caused by stronger entrainment and subsequent BL collapse during day 1 of the N_d=100 cm^{-3} runs.

moisture transport from the surface, hinted at by decreased w_* in Fig. 13f.

It is interesting to note that the more weakly-entraining cases are better able to maintain cloud towards the end of the run. This is because z_i is much lower in these runs, making it easier to keep the BL well-mixed. This behavior reaffirms that we can associate decreased entrainment with longer cloud lifetime (as suggested by Stevens et al., 1998, and others).

Fig. 16 shows the timeseries of observed N_d and the timeseries of $F_P(0)$, LWP, and z_i from a 2D run forced by these droplet concentrations. As noted above, entrainment tends to be higher and drizzle tends to be lower for larger N_d. The LWP timeseries can largely be explained by superposition of these effects.

5 Conclusions

In this study, we were able to reproduce many of the observed features from the EPIC-Sc dataset using the SAM LES. In particular, the model was able to reproduce the mean q_t and s_l budgets very well and to capture the observed BL stratification. In addition, the diurnal cycle of LWP was well-simulated, although this appears to be partially the result of canceling errors in z_i and z_b.

A surprising result of this study is that model entrainment appears to closely follow the relation $w_e = w_* \mathrm{Ri}^{-1}$ found in C05 even though comparison of the diurnal cycle of w_e and z_i suggests that the LES underpredicts the amplitude of the diurnal cycles of these quantities. The explanation for this seeming paradox is that while the observations fit the

above relation most of the time, the midday w_e is significantly less than that predicted by the $w_* \mathrm{Ri}^{-1}$ relation. This suggests that entrainment observations are underestimated at this time in the observations or that the processes governing midday entrainment are different than those operating at other times.

Comparison between radar-derived precipitation profiles and the profiles generated by the Khairoutdinov and Kogan (2000) scheme suggest that the model is too sensitive to LWP and that evaporation of drizzle below cloud base is underpredicted.

Since the model was able to reproduce most of the observed aspects of the BL sampled during EPIC, it is a useful tool for understanding BL properties not captured during the EPIC cruise. Vertical velocity variance (which was measured during the cruise but hasn't been processed) is one such quantity. Profiles of this quantity from the model typically had a double-peaked profile and below cloud base intermittent pulsing of turbulence was common. These suggest that the LES is maintaining a marginally-decoupled state much of the time, even when it is is relatively well-mixed as measured by vertical moisture stratification. Correlation between $\overline{w'w'}$ and w_e for various heights in the BL suggests that the typical depth of entraining eddies in the model is less than 0.4 times the BL depth, which suggests that a transfer function between buoyancy flux and entrainment which is weighted more towards cloud top is probably superior to the BL average commonly used.

Sensitivity studies were also performed to investigate the importance of subsidence and drizzle to BL dynamics. Removing the diurnal cycle of subsidence resulted in weaker

diurnal variation in cloud top. This change had little impact on the LWP due to compensating variations in cloud base. Two sensitivity studies were performed to assess the importance of drizzle. In one study, autoconversion is turned off, preventing the formation of drizzle. This results in much stronger daily-maximum LWP and resultingly stronger SW cloud forcing during the early morning and late afternoon but had little effect on daily minimum LWP. Surprisingly, BL depth was almost entirely unaffected by eliminating drizzle as long as cloud droplet sedimentation is left unaltered. However, when droplet concentration was decreased to 25 cm^{-3} (a factor of 4 decrease), entrainment was substantially decreased and LWP was substantially reduced from the control run. This w_e difference appears to be the result of increased droplet sedimentation associated with dividing cloud-top liquid water into fewer drops. On the other hand, simulation-mean cloud fraction was substantially enhanced in this run due to the improved ability for the BL to mix associated with decreased z_i.

This study provides hope that LES simulations of the diurnal cycle of Sc are not only possible but also illuminating. Better understanding of how to handle model overentrainment and the computational resources to simulate a larger region less susceptible to domain-scale convective pulsing would also aid our understanding.

Acknowledgments

Much gratitude is due to Marat Khairoutdinov for supplying us with SAM and the KK drizzle scheme, and to Peter Blossey and Marc Michelson for assistance in implement-

ing these codes at the UW. Thanks is also due to Rob Wood and Dennis Hartmann for their thoughtful comments on this manuscript. This research was funded by as funded by NSF grant ATM-0433712, with computer resources provided through NASA grant NNG05GA19G. Part of this work was performed under the auspices of the U.S. Department of Energy by Lawrence Livermore National Laboratory under Contract DE-AC52-07NA27344.

Appendix: Surface Geostrophic Winds

Assuming $Du/Dt = 0$ and neglecting viscous effects, the Boussinesq momentum equations can be written

$$f\left(v - v_g\right) = \frac{\partial \overline{u'w'}}{\partial z}, \tag{1}$$

$$-f\left(u - u_g\right) = \frac{\partial \overline{v'w'}}{\partial z} \tag{2}$$

where v_g and u_g are the zonal and meridional geostrophic winds, respectively. If the BL is well-mixed, u, v, u_g, and v_g should be constant in height above the surface layer. Assuming the momentum flux across z_i to be zero (reasonable since $w' \approx 0$ above z_i), (1) and (2) can be integrated between 0 and z_i to yield

$$v_g = v + \frac{\overline{u'w'}(0)}{f z_i} \tag{3}$$

$$v_g = u - \frac{\overline{v'w'}(0)}{f z_i}. \tag{4}$$

To compute representative values for EPIC from the above equations, u and v are taken to be BL-average values from radiosonde data. Surface momentum fluxes are computed using ship-based 14 m winds and the empirical relation

$$\overline{\mathbf{u}'w'}(0) = -C_D \left|\mathbf{u}\right| \mathbf{u} \tag{5}$$

with $C_D = 1.5 \times 10^{-3}$.

References

Ackerman, A. S., M. Kirkpatrick, D. Stevens, and O. Toown, 2004: The impact of humidity above stratiform clouds on indirect aerosol climate forcing. *Nature*, 1014–1017, doi:10.1038/nature03174.

Ackerman, A. S. et al., 2008: Large-eddy simulations of a drizzling, stratocumulus-topped marine boundary layer, submitted Mon. Weath. Rev. 3/08.

Bony, S. and J.-L. Dufresne, 2005: Marine boundary layer clouds at the heart of cloud feedback uncertainties in climate models. *J. Geophys. Res.*, **32**, L20806, doi: 10.1029/2005GL023851.

Bretherton, C., P. Blossey, and J. Uchida, 2007: Cloud droplet sedimentation, entrainment efficiency, and subtropical stratocumulus albedo. *Geophys. Res. Lett.*, **34**, L03813, doi: 10.1029/2006GL027648.

Bretherton, C. S., M. MacVean, P. Bechtold, A. Chlond, W. Cotton, J. Cuxart, H. Cuijpers, M. Khairoutdinov, D. Lewellen, C. Moeng, P. Siebesma, B. Stevens, D. Stevens, I. Sykes, and M. Wyant, 1999: An intercomparison of radiatively driven entrainment and turbulence in a smoke cloud, as simulated by different numerical models. *Quart. J. Roy. Meteor. Soc.*, **125**, 391–423.

Bretherton, C. S., T. Uttal, C. W. Fairall, S. E. Yuter, R. A. Weller, D. Baumgardner,

K. Comstock, and R. Wood, 2004: The EPIC 2001 stratocumulus study. *Bull. Amer. Meteor. Soc.*, **85**, 967–977.

Collins, W. et al., 2006: The Community Climate System Model: CCSW3. *J. Climate*, **19**, 2122–2143.

Comstock, K., R. Wood, S. E. Yuter, and C. S. Bretherton, 2004: Reflectivity and rain rate in and below drizzling stratocumulus. *Quart. J. Roy. Meteor. Soc.*, **130**, 2891–2918.

Deardorff, J., 1980: Stratocumulus-capped mixed layers derived from a three-dimensional model. *Bound.-Layer Meteor.*, **18**, 495–527.

deSzoeke, S. P. and C. S. Bretherton, 2004: Quasi-Lagrangian Large Eddy Simulations of Cross-Equatorial Flow in the East Pacific Atmospheric Boundary Layer. *J. Atmos. Sci.*, **61**, 1837–1858.

Duynkerke, G. P., R. S. de Roode, C. van Zanten Margreet, J. Calvo, J. Cuxart, S. Cheinet, A. Chlond, H. Grenier, P. J. Jonker, M. Köhler, G. Lenderink, D. Lewellen, C.-L. Lappen, P. A. Lock, C.-H. Moeng, F. Müller, D. Olmeda, J.-M. Piriou, E. Sánchez, and I. Sednev, 2004: Observations and numerical simulations of the diurnal cycle of the EUROCS stratocumulus case. *Quart. J. Roy. Meteor. Soc.*, **130**, 3269–3296.

Germano, M., U. Piomelli, P. Moin, and W. Cabot, 1991: A dynamic subgrid-scale eddy viscosity model. *Phys. Fluids A*, **3**, 1760–1765.

Khairoutdinov, M. F. and Y. L. Kogan, 2000: A new cloud physics parameterization in a large-eddy simulation model of marine stratocumulus. *Mon. Wea. Rev.*, **128**, 229–243.

Khairoutdinov, M. F. and D. A. Randall, 2003: Cloud resolving modeling of the ARM summer 1997 IOP: model formulation, results, uncertainties, and sensitivities. *J. Atmos. Sci.*, **60**, 607–625.

Klein, S. A. and D. L. Hartmann, 1993: The seasonal cycle of low stratiform clouds. *J. Climate*, **6**, 1587–1606.

Lewellen, D. and W. Lewellen, 1998: Large-eddy boundary layer entrainment. *J. Atmos. Sci.*, **55**, 2645–2665.

Lilly, D., 2002: Entrainment into mixed layers. Part II: A new closure. *J. Atmos. Sci.*, 3353–3361.

Lock, A., 1998: The parameterization of entrainment in cloudy boundary layers. *Quart. J. Roy. Meteor. Soc.*, **124**, 2729–2753.

Martin, G. M., W. Johnson, and A. Spice, 1994: The measurement and parameterization of effective radius of droplets in warm stratocumulus clouds. *J. Atmos. Sci.*, **51**, 1823–1842.

Moeng, C.-H., 2000: Entrainment rate, cloud fraction, and liquid water path of PBL stratocumulus clouds. *Journal of Atmospheric Sciences*, **57**, 3627–3643.

Nigam, S., 1997: The annual warm to cold phase transition in the eastern equatorial Pacific: Diagnosis of the role of stratus cloud-top cooling. *J. Climate*, **10**, 2447–2467.

Paluch, I. R. and D. H. Lenschow, 1991: Stratiform cloud formation in the marine boundary layer. *J. Atmos. Sci.*, **48**, 2141–2158.

Pawlowska H. and J.-L. Brenguier, 2003: An observational study of drizzle formation in stratocumulus clouds for general circulation model (GCM) parameterizations. *J. of Geophys. Res. (Atmospheres)*, **108**, 8630–+.

Pope, S., 2000: *Turbulent Flows*. Cambridge University Press, 770pp.

Savic-Jovcic, V. and B. Stevens, 2007: The structure and mesoscale organization of precipitating stratocumulus, submitted, J. Atmos. Sci.

Smagorinsky, J., 1963: General circulation experiments with the primitive equations: I. the basic equations. *Mon. Weather Rev.*, **91**, 99–164.

Stevens, B., 2002: Entrainment in stratocumulus-topped mixed layers. *Quart. J. Roy. Meteorol. Soc.*, **128**, 2663–2689.

Stevens, B., W. R. Cotton, G. Feingold, and C.-H. Moeng, 1998: Large-eddy simulations of strongly precipitating, shallow stratocumulus-topped boundary layers. *J. Atmos. Sci.*, **55**, 3616–3638.

Stevens, B., C.-H. Moeng, and P. P. Sullivan, 1999: Large-Eddy Simulations of Ra-

diatively Driven Convection: Sensitivities to the Representation of Small Scales. *J. Atmos. Sci*, **56**, 3963–3984.

Stevens, B., G. Vali, K. Comstock, R. Wood, M. vanZanten, P. Austin, C. Bretherton, and D. Lenschow, 2005a: Pockets of open cells and drizzle in marine stratocumulus. *Bull. Amer. Meteor. Soc.*, 51–57.

Stevens, B. et al., 2005b: Evaluation of large-eddy simulations via observations of nocturnal marine stratocumulus. *Mon. Wea. Rev.*, **133**, 1443–1462.

Stevens, D. E. and C. S. Bretherton, 1999: Effects of resolution on the simulation of stratocumulus entrainment. *Quart. J. Roy. Meteorol. Soc.*, **125**, 425–439.

Turton, J. and S. Nicholls, 1987: A study of the diurnal variation of stratocumulus using a multiple mixed layer model. *Q.J.R. Meteorol. Soc*, **113**, 969–1009.

vanZanten, M., P. Duynkerke, and W. Cuijpers, 1999: Entrainment parameterizations in convective boundary layers derived from large eddy simulations. *J. Atmos. Sci.*, **56**, 813–828.

Vanzanten, M. C., B. Stevens, G. Vali, and D. H. Lenschow, 2005: Observations of Drizzle in Nocturnal Marine Stratocumulus. *Journal of Atmospheric Sciences*, **62**, 88–106.

Wood, R., 2005: Drizzle in stratocumulus clouds. Part I: Aircraft observations. *J. Atmos. Sci.*, **62**, 3011–3033.

Xue, H., G. Feingold, and B. Stevens, 2007: Aerosol effects on clouds, precipitation, and the organization of shallow cumulus convection, accepted.

Yu, J.-Y. and C. R. Mechoso, 1999: Links between Annual Variations of Peruvian Stratocumulus Clouds and of SST in the Eastern Equatorial Pacific. *Journal of Climate*, **12**, 3305–3318.

List of Figures

7 Profiles of $\overline{w'w'}$ from the 3d control run. Each profile is computed by averaging over the domain and over the 3 hr period centered at the time noted on the legend. 47

8 Timeseries of TKE budget terms from 3D base simulation (in m^2 s^{-3}). Storage (negligibly small) is omitted. Nighttime values are indicated by black lines along the base of panel (a). 48

9 (a). Relation between w_e and $\overline{w'w'}$ for 3D base simulation and (b) relation between w_e and buoyancy driving (following Fig. 11 of C05). In each panel, model values are dots and observations are pluses. Daytime values are light gray and nighttime values are dark gray except for the diurnal mean observations in panel (b), which are all colored black. 49

10 Comparison between composite diurnal cycle of w_e (solid lines) and $w_* \mathrm{Ri}^{-1}$ (dashed lines) for model (gray) and observations (black). The diurnal cycle has been repeated twice for clarity. 50

11 Correlation between domain-averaged values of entrainment and $\overline{w'w'}$ (panel (a)) or buoyancy flux (panel (b)) calculated at various fractions of the BL depth from the 3d control run. 51

Table 1: Mean and standard deviation for each term in the q_t budget from the 3D control run. Terms are derived and signed following the C05 conventions. Mean values from C05 are included here for convenience.

	$-\frac{L\hat{p}_i}{g}\frac{\partial\langle q_t\rangle}{\partial t}$	$-\frac{L\hat{p}_i}{g}\langle \mathbf{v}\cdot\nabla_h q_t\rangle$	LHF	$LF_p(0)$	$\frac{L}{g}\hat{\omega}_e\Delta q_t$	Residual
Obs Mean:	-6	-26	99	-5	-68	-6
LES Mean:	1	-27	108	-4	-75	3
LES St. Dev:	6	6	3	1	4	1

Table 2: As for Table 1, but for the s_l budget.

	$-\frac{\hat{p}_i}{g}\frac{\partial\langle s_l\rangle}{\partial t}$	$-\frac{\hat{p}_i}{g}\langle \mathbf{v}\cdot\nabla_h s_l\rangle$	SHF	$-LF_p(0)$	$-\Delta_{\mathrm{BL}}F_R$	$\frac{1}{g}\hat{\omega}_e\Delta s_l$	Residual
Obs Mean:	1	-19	14	5	-52	41	-10
LES Mean:	-2	-20	13	4	-46	53	2
LES St. Dev:	4	3	1	1	2	3	3

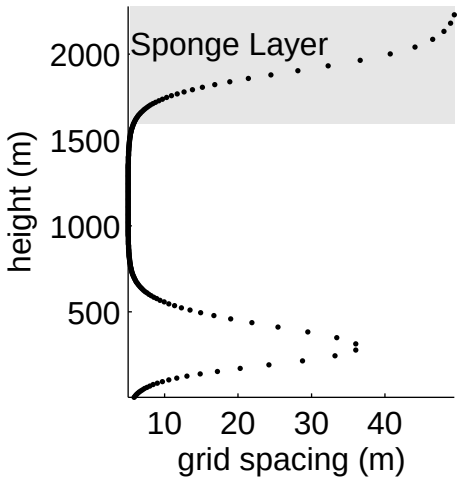

Figure 1: Vertical grid spacing for SAM runs. The sponge region is shaded.

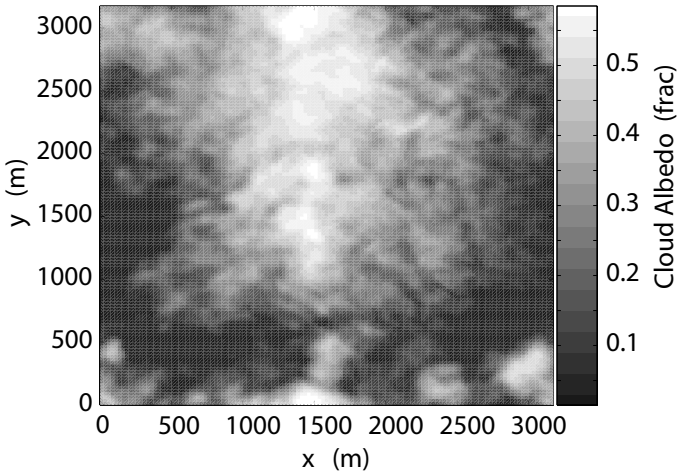

Figure 2: Snapshot of cloud albedo (calculated following Savic-Jovcic and Stevens (2007)) at 32 hrs into run (0400 LT).

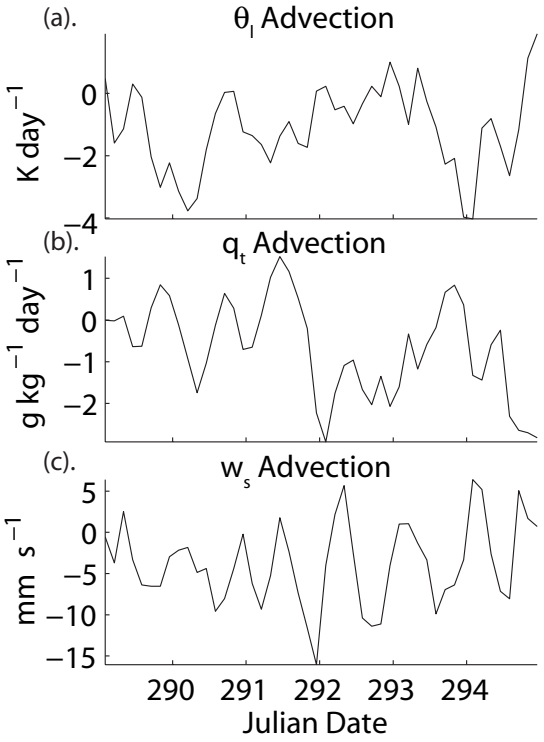

Figure 3: Advection (assumed uniform in height) and 850mb subsidence used to force the LES simulations. Subsidence does not include the $-\mathbf{v} \cdot \nabla_h z_i$ correction.

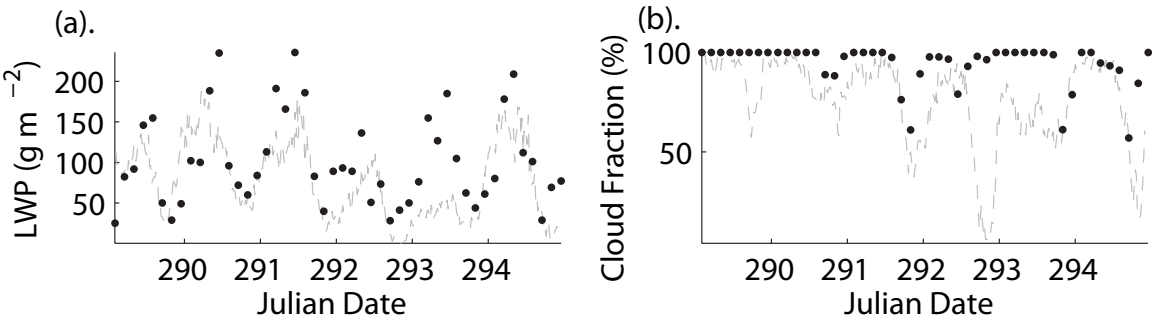

Figure 4: Timeseries of (a) LWP and (b) cloud fraction from the 3D base simulation (dashed line) and the observations (dots).

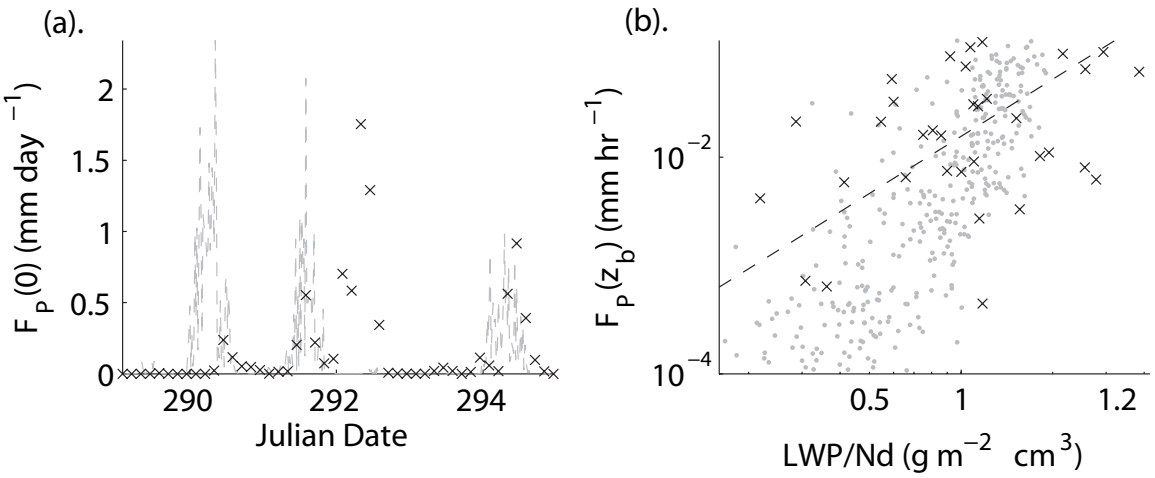

Figure 5: (a) Timeseries of surface drizzle from base simulation (gray line) and as observed by C-band radar (black crosses). (b) Comparison of control-simulation cloud base drizzle rates (gray dots) with values computed from the 5 cm scanning radar (black crosses) and with the empirical relation to LWP and N_d derived in Comstock et al. (2004) (black dashed line).

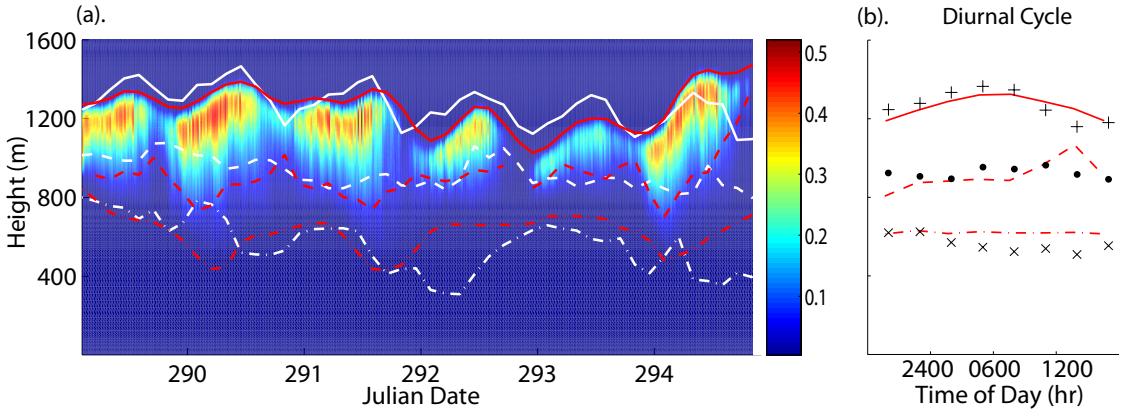

Figure 6: (a) Timeseries of model q_l in g kg^{-1} (color) along with model (red) and observations (white) of z_i (solid lines), z_b (dashed lines), and LCL (dot-dashed lines). (b) Diurnal cycle of z_i, z_b, and LCL. Color and linestyle for model are as in (a) while observations are in black pluses, dots, and xs, respectively.

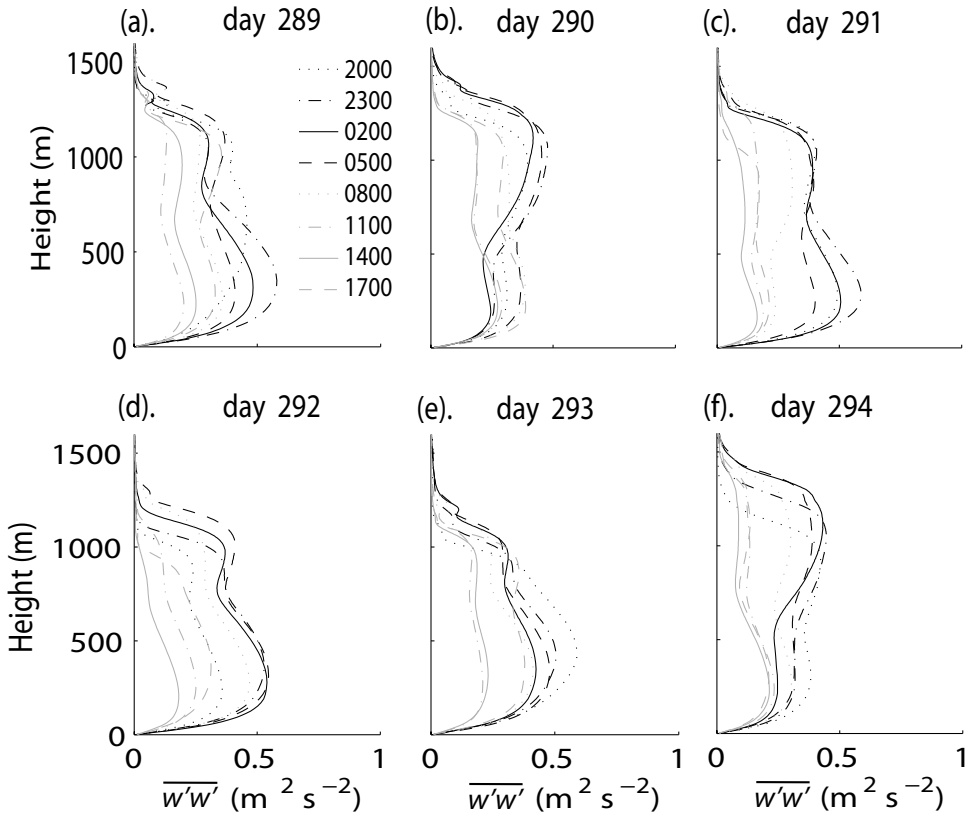

Figure 7: Profiles of $\overline{w'w'}$ from the 3d control run. Each profile is computed by averaging over the domain and over the 3 hr period centered at the time noted on the legend.

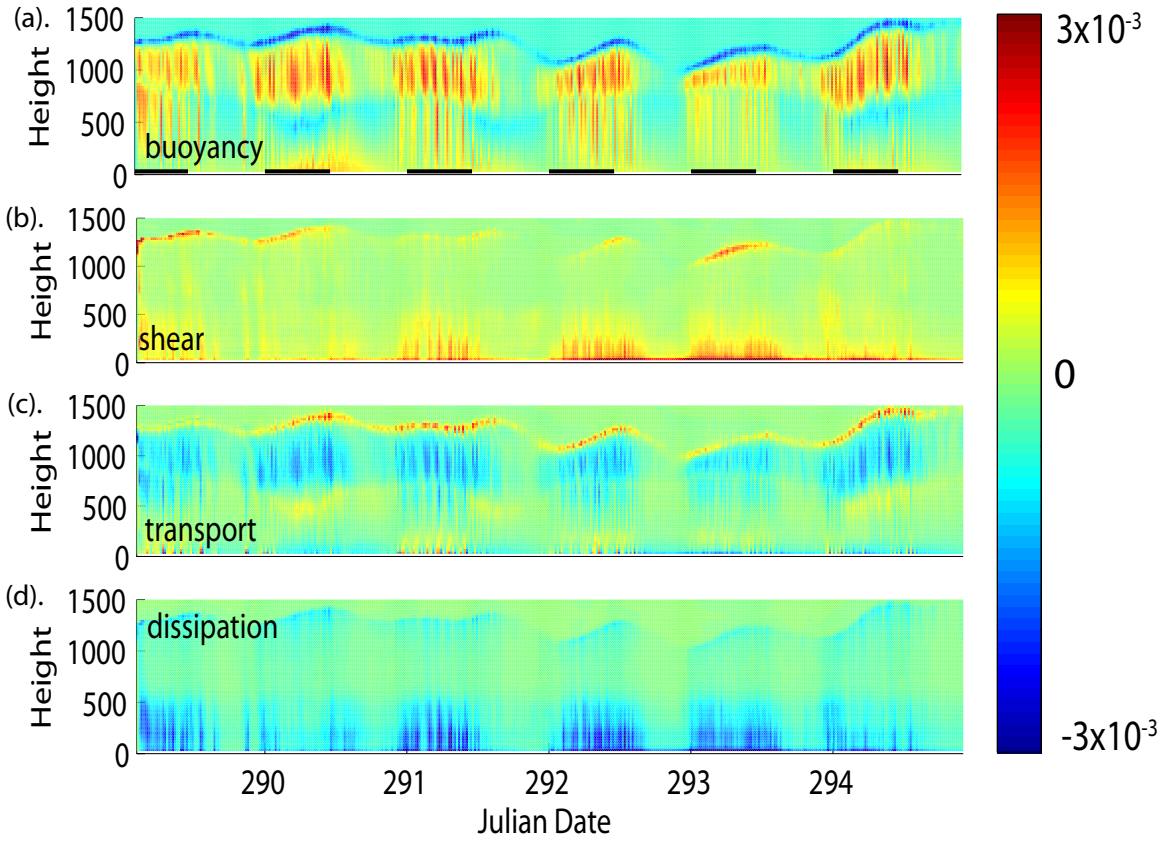

Figure 8: Timeseries of TKE budget terms from 3D base simulation (in $m^2\ s^{-3}$). Storage (negligibly small) is omitted. Nighttime values are indicated by black lines along the base of panel (a).

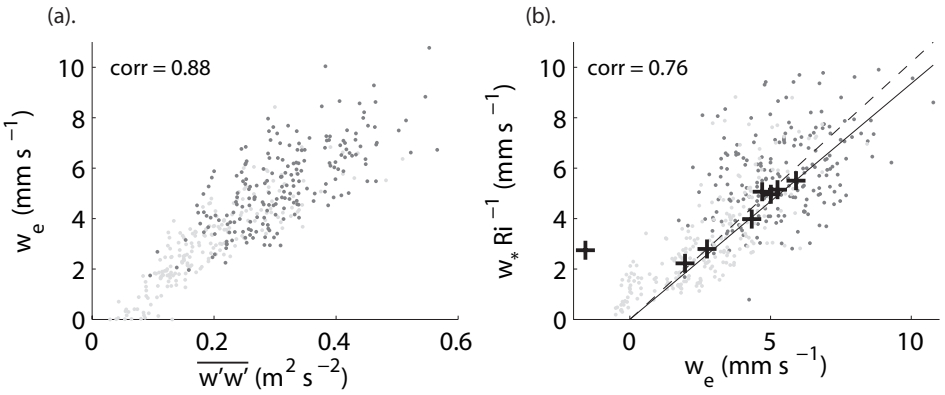

Figure 9: (a). Relation between w_e and $\overline{w'w'}$ for 3D base simulation and (b) relation between w_e and buoyancy driving (following Fig. 11 of C05). In each panel, model values are dots and observations are pluses. Daytime values are light gray and nighttime values are dark gray except for the diurnal mean observations in panel (b), which are all colored black.

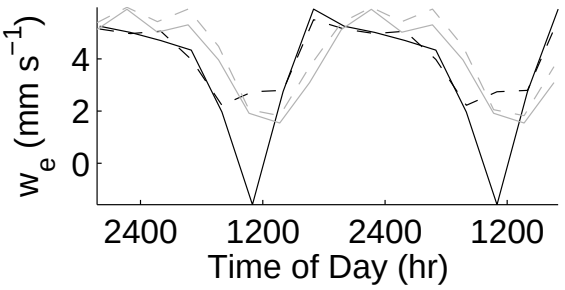

Figure 10: Comparison between composite diurnal cycle of w_e (solid lines) and $w_* \mathrm{Ri}^{-1}$ (dashed lines) for model (gray) and observations (black). The diurnal cycle has been repeated twice for clarity.

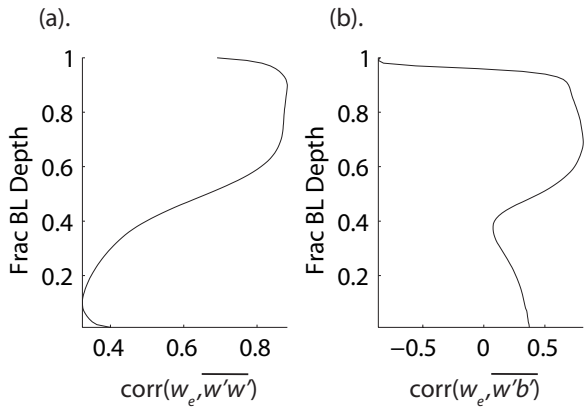

Figure 11: Correlation between domain-averaged values of entrainment and $\overline{w'w'}$ (panel (a)) or buoyancy flux (panel (b)) calculated at various fractions of the BL depth from the 3d control run.

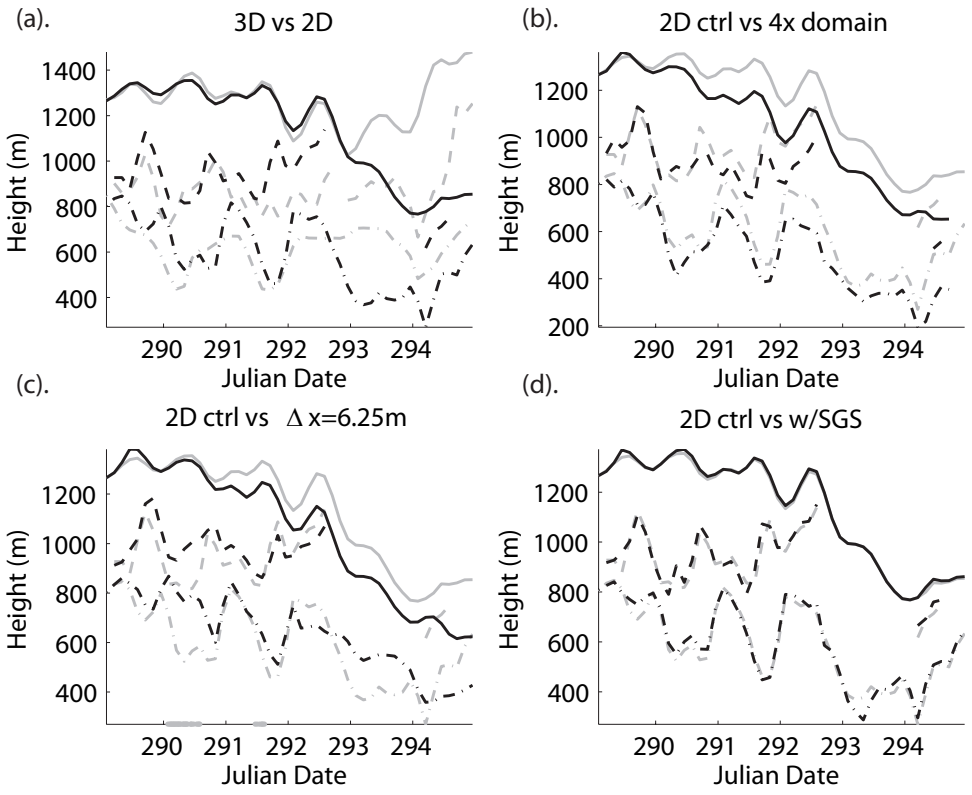

Figure 12: Comparison of z_i, z_b, and LCL from (a) 3D versus 2D base simulations, (b) 2D base simulation versus a similar simulation with 4 times larger domain, (c) 2D base simulation versus a similar simulation with $\Delta x = 6.25$ m, and (d) 2D base simulation versus 2D simulation with scalar SGS fluxes computed using Smagorinsky. In panel (c), times of surface drizzle > 0.25 mm day^{-1} are indicated by dots near the bottom of the plot. In all plots, the first run mentioned is shown in gray, the second in black.

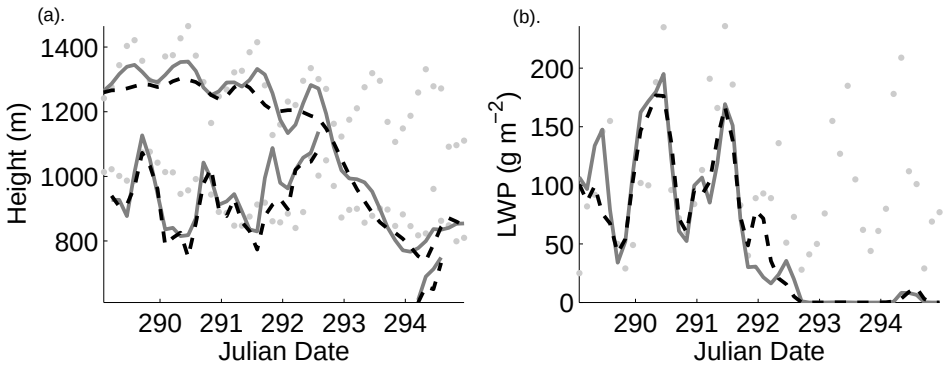

Figure 13: Timeseries of (a) z_i and z_b and (b) LWP from observations (dots), from the 2D base simulation (solid lines), and from a run forced by the 24 hr running mean of the observed w_s (dashed lines).

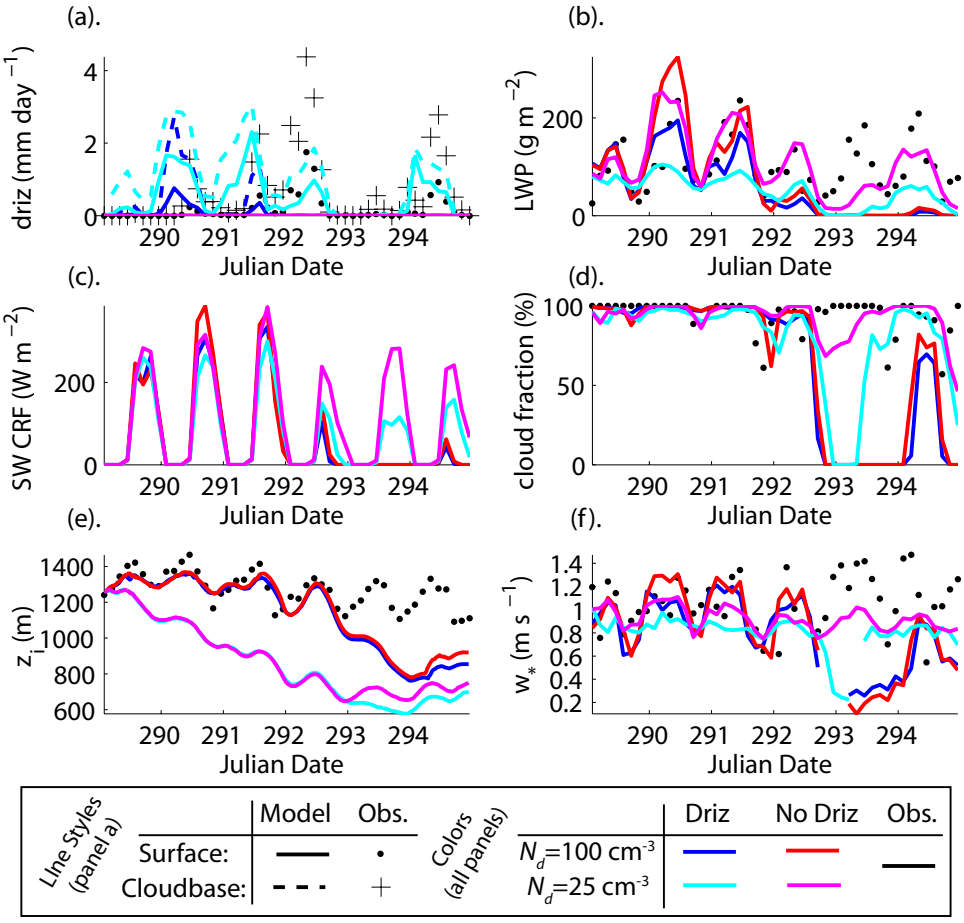

Figure 14: Effect of drizzle on 2D simulations.

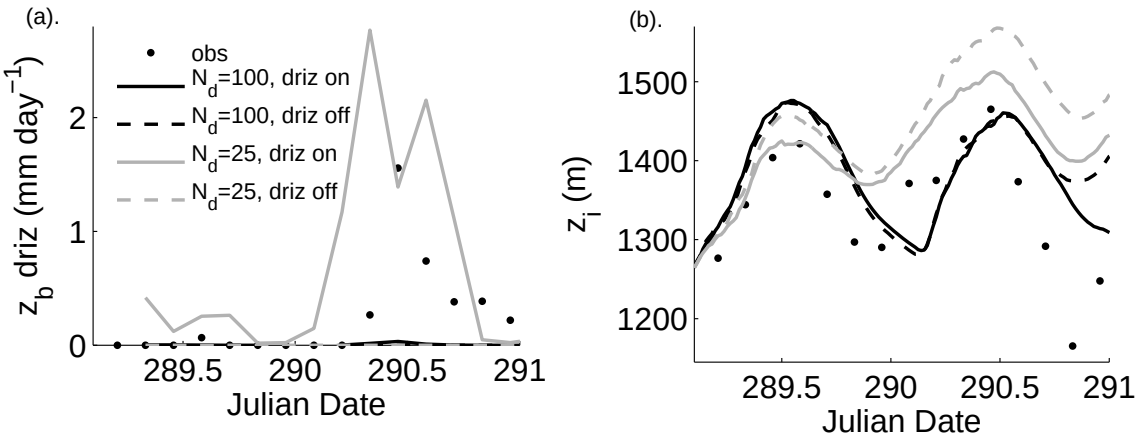

Figure 15: Cloud base drizzle (panel (a)) and z_i (panel (b)) from simulations using $\sigma_g = 1.2$.

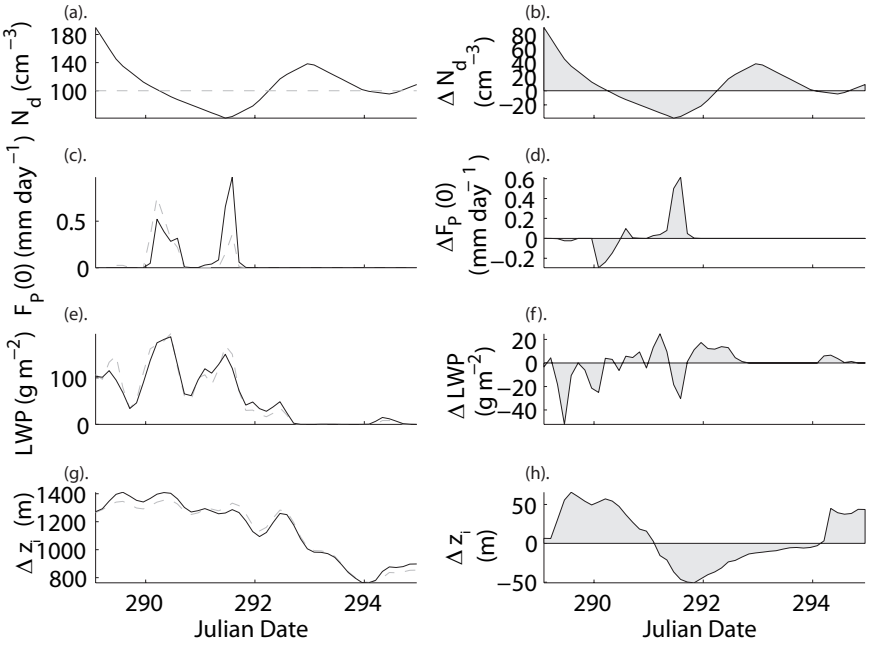

Figure 16: (a)-(b) Droplet concentration, (c)-(d) surface drizzle rate, (e)-(f) LWP, and (g)-(h) z_i from (1) the varying N_d run (black solid line) and (2) the 2D control simulation (dashed gray line). Panels on the right show the difference between the N_d-varying and control simulation.